

Tree-ring cellulose $\delta^{18}\text{O}$ records similar large-scale climate influences as precipitation $\delta^{18}\text{O}$ in the Northwest Territories of Canada

Robert D. Field¹ · Laia Andreu-Hayles^{2,3,4} · R. D. D'arrigo² · R. Oelkers² · B. H. Luckman⁵ · D. Morimoto⁵ · E. Boucher⁶ · F. Gennaretti⁷ · I. Hermoso⁶ · A. Lavergne⁸ · M. Levesque⁹

Received: 5 February 2021 / Accepted: 10 August 2021 / Published online: 24 October 2021 © The Author(s), under exclusive licence to Springer-Verlag GmbH Germany, part of Springer Nature 2021, corrected publication 2021

Abstract

Stable oxygen isotopes measured in tree rings are useful for reconstructing climate variability and explaining changes in physiological processes occurring in forests, complementing other tree-ring parameters such as ring width. Here, we analyzed the relationships between different climate parameters and annually resolved tree-ring $\delta^{18}O$ records ($\delta^{18}O_{TR}$) from white spruce (*Picea glauca* [Moench]Voss) trees located near Tungsten (Northwest Territories, Canada) and used the NASA GISS ModelE2 isotopically-equipped general circulation model (GCM) to better interpret the observed relationships. We found that the $\delta^{18}O_{TR}$ series were primarily related to temperature variations in spring and summer, likely through temperature effects on the precipitation $\delta^{18}O$ in spring, and evaporative enrichment at leaf level in summer. The GCM simulations showed significant positive relationships between modelled precipitation $\delta^{18}O$ over the study region and surface temperature and geopotential height over northwestern North America, but of stronger magnitudes during fall-winter than during spring–summer. The modelled precipitation $\delta^{18}O$ was only significantly associated with moisture transport during the fall-winter season. The $\delta^{18}O_{TR}$ showed similar correlation patterns to modelled precipitation $\delta^{18}O$ only during spring–summer when water matters more for trees, with significant positive correlations with surface temperature and geopotential height, but no correlations with moisture transport. Overall, the $\delta^{18}O_{TR}$ records for northwestern Canada reflect the same significant large-scale climate patterns as precipitation $\delta^{18}O$ for spring–summer, and therefore have potential for reconstructing past atmospheric dynamics in addition to temperature variability in the region.

Keywords Paleoclimate · Stable isotopes · Dendrochronology · General circulation models · NASA GISS Model E2 · Snow

Robert D. Field and Laia Andreu-Hayles contributed equally to this work.

- Robert D. Field robert.field@columbia.edu
- ☐ Laia Andreu-Hayles lah@ldeo.columbia.edu
- Department of Applied Physics and Applied Mathematics, NASA Goddard Institute for Space Studies, Columbia University, New York, NY, USA
- Tree-Ring Laboratory, Lamont-Doherty Earth Observatory of Columbia University, Palisades, NY 10964, USA
- ³ CREAF, Bellaterra (Cerdanyola del Vallés), Barcelona, Spain
- ⁴ ICREA, Pg. Lluís Companys 23, Barcelona, Spain
- Department of Geography, University of Western Ontario, London, Canada

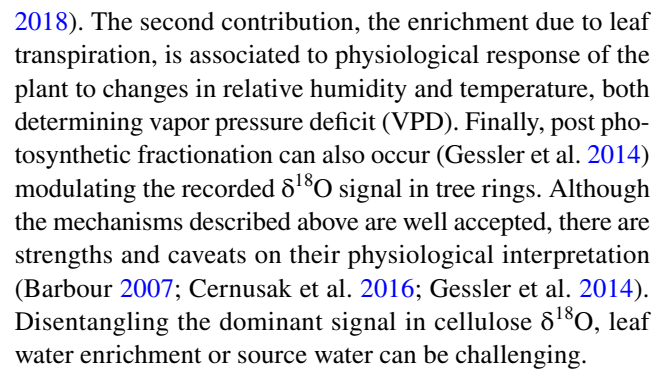
- Department of Geography, GEOTOP, and Centre d'études nordiques, University of Québec at Montréal, Montreal H2X 3R9, Canada
- Institut de Recherche sur les Forêts, Groupe de Recherche en Écologie de la MRC Abitibi, UQAT, Amos, Quebec J9T 2L8, Canada
- ⁸ Carbon Cycle Research Group, Space and Atmospheric Physics, Department of Physics, Imperial College London, London SW7 2AZ, UK
- Forest Management Group, Department of Environmental Systems Science, ETH Zurich, 8092 Zurich, Switzerland



1 Introduction

Tree rings have been used to reconstruct climate, particularly temperature, over northwestern North America prior to the instrumental period, primarily using tree-ring width (TRW) and maximum latewood density (MXD) data for the past millennium (Anchukaitis et al. 2012; Briffa et al. 2004; D'Arrigo et al. 2014). Such records have also been used to generate indices of patterns of large-scale atmosphericocean circulation, such as the Aleutian Low, or the Pacific Decadal Oscillation (PDO) for the north Pacific sector (e.g. D'Arrigo et al. 2001; Gaglioti et al. 2019; Villalba et al. 2011). Tree-ring density proxies such as MXD have been shown to have a more stable and robust temperature signal than ring-width chronologies from the same trees, and thus have been used to generate temperature reconstructions for a variety of northern sites, e.g. in British Columbia (Wilson and Luckman 2003), at latitudinal treeline at Firth River in Alaska (Anchukaitis et al. 2012; Andreu-Hayles et al. 2011a) and in the Yukon (Morimoto 2015), as well as for the Northern Hemisphere (Anchukaitis et al. 2017; Wilson et al. 2016). Blue intensity (BI), a novel proxy for density, has been used to produce reconstructions in Yukon (Wilson et al. 2019) and the Gulf of Alaska (Wilson et al. 2017), among other locations.

The isotopic composition of stable oxygen (δ^{18} O, ratio of ¹⁸O-¹⁶O relative to a standard) measured in cellulose from tree rings can be used as another climate proxy and can provide complementary and unique information relative to TRW and MXD/BI data. This isotopic information includes, for example, physiological insights into tree response to environmental changes in boreal and other terrestrial ecosystems (e.g. Andreu-Hayles et al. 2011b; Barber et al. 2000; Levesque et al. 2017), information about the source water used by the tree (e.g. Gessler et al. 2014; McCarroll and Loader 2004), and climate variability (e.g. Andreu-Hayles et al. 2017; Gennaretti et al. 2017). The δ^{18} O signature recorded in tree rings mostly results from (1) the isotopic composition of the source water that is taken up by the roots; (2) the isotopic enrichment occurring due to leaf transpiration; and (3) the isotopic exchange of oxygen atoms between cellulose and xylem water when cellulose is formed. The first and the third contributions are related to the water source signal of precipitation δ^{18} O and isotopic balance in the soil (Dansgaard 1964). Precipitation δ^{18} O can vary regarding the trajectory of the air masses, the distance from the original source and their exposure to warmer/colder atmospheric conditions that will determine the amount of moisture that can be held and the number of rainouts (i.e. depleting the original δ^{18} O signature) before arriving to the studied trees. The δ^{18} O of source water can also vary due to the use of water pools from different soil depths (Barbeta et al. 2020; Brinkmann et al.



Because tree-ring $\delta^{18}O$ ($\delta^{18}O_{TR}$) records are affected by climate variability, they can be a powerful additional proxy for reconstructing atmospheric circulation patterns for centuries prior to the instrumental period (Balting et al. 2021: Szejner et al. 2016). Understanding the linkages between $\delta^{18}O_{TR}$ and precipitation $\delta^{18}O$ is also important for improving past climate reconstructions in these high-latitude boreal regions (Anchukaitis et al. 2017; D'Arrigo et al. 2014; Wilson et al. 2016). In the extratropical regions of the Northern Hemisphere, precipitation δ^{18} O is strongly related to temperature (Birks and Edwards 2009). This relationship is in part reflected in the positive correlations typically seen between $\delta^{18}O_{TR}$ and temperature, and in theory may be attributable to large-scale atmospheric circulation patterns that prevail in this area. For example, summer temperatures were reconstructed over the last millennium using $\delta^{18}O_{TR}$ records (Naulier et al. 2015), and annual temperatures and δ¹⁸O meteoric water values were estimated from Pleistocene subfossil wood from Bylot Island, Canada (Csank et al. 2013). In the southern Yukon, an atmospheric general circulation model equipped with stable water isotope tracers demonstrated that high δ^{18} O values in meteoric water were associated with an intensified Aleutian Low pressure cell, bringing stronger southerly moisture flow to eastern Alaska and the southern Yukon (Field et al. 2010). Such general circulation models can provide an idealized picture of the climatic influence on local precipitation δ^{18} O (Field et al. 2010; Porter et al. 2014) in the absence of long-term precipitation δ^{18} O records.

Determination of the climate signal in $\delta^{18}O_{TR}$ requires comparisons with observed climate variables, typically obtained from nearby meteorological stations. In prior work, Begin et al. (2015) and Naulier et al. (2015) identified summer maximum temperature and VPD influences on black spruce $\delta^{18}O_{TR}$ for a site in north-central Quebec using weather station data from three stations 100–300 km away, each with data available for roughly 50 years. Holzkamper et al. (2012) reported a robust relationship between spring temperature and precipitation with white spruce $\delta^{18}O$ at a site in Nunavut over the 1986–2004 interval for a weather station roughly 300 km away. Csank et al. (2016) documented spring-summer climatic controls on $\delta^{18}O$ using



Global Historical Climate Network (GHCN) stations within 100 km of sampling sites in south-coastal Alaska between 1949 and 2011.

Station records are typically few, very limited across space and have short or incomplete records in remote regions such as those studied herein (e.g. Holzkamper et al. 2012), making it difficult to identify robust local or large-scale climatic influences. Gridded observational products and meteorological reanalysis are, in theory, an alternative, and can also help to identify regional influences on tree-ring signals. For example, gridded climate products have been used for reconstructing summer temperatures (Gennaretti et al. 2017) and streamflow (Brigode et al. 2016) in northern Quebec.

Here, our objective is to assess the climate signal and atmospheric circulation patterns associated with inter-annual variations in a newly-developed alpha-cellulose-derived $\delta^{18}O_{TR}$ chronology for a site located in the Northwest Territories, Canada, and thus determine the potential of these records to reconstruct large-scale climate variability in the region. We focus specifically on how these relationships are detected in several different types of datasets, namely: (i) homogenized station records and 'raw' station records with additional parameters, (ii) two gridded temperature datasets estimated from meteorological station data but using different interpolation techniques, and (iii) two meteorological reanalyses. We also use an isotopically-equipped general

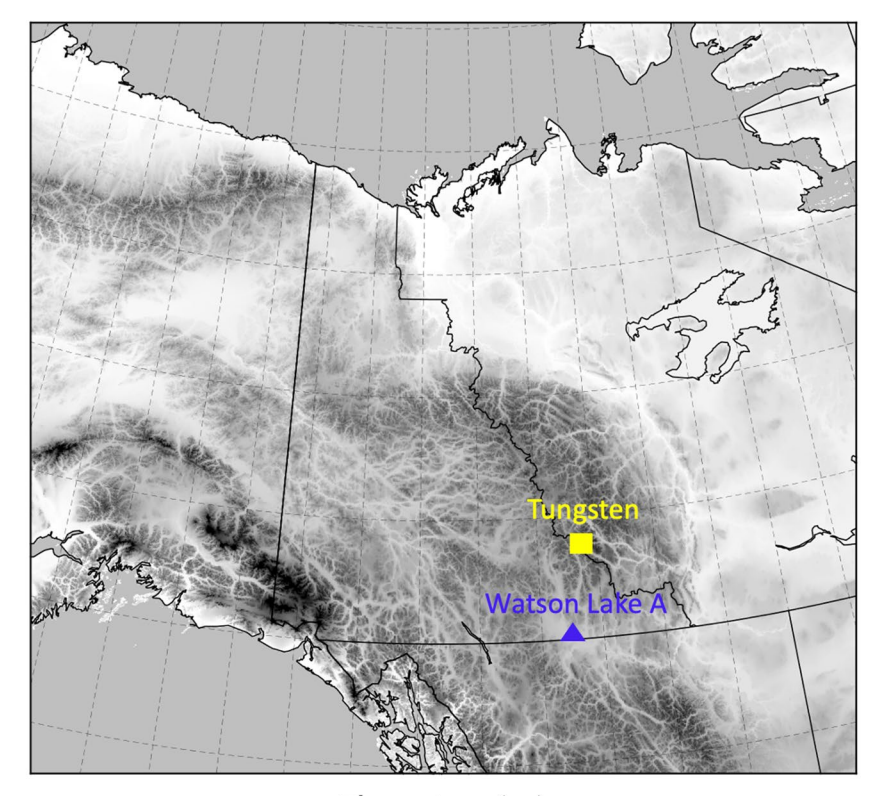
Fig. 1 Location of the treering chronology at Tungsten (61.98° N; 128.25° W) and the Watson Lake Global Historical Climatological Network (GHCN) weather station (60.117 °N, 128.817 °W)

circulation model (GCM) to understand climatic controls on local precipitation $\delta^{18}O,$ and to help interpret the different seasonal relationships identified between $\delta^{18}O_{TR}$ and the climate observations. Overall, we aimed to determine the potential of using tree-ring $\delta^{18}O$ to reconstruct large-scale climate indicators interpreting what climatic signals might be detectable using a broad range of data and GCM simulations. Our interest in this region is motivated by the need to provide context prior to the instrumental period for north Pacific climate variability and high-latitude climate change.

2 Data and methods

2.1 Tree-ring data

The tree-ring samples were collected from white spruce (*Picea glauca* [Moench]Voss) located at 1145 m a.s.l near Tungsten (61.98° N; –128 to 25° W; Fig. 1), Northwest Territories (NWT), Canada in the year 2003 (Morimoto 2015). The sampled stand consisted of isolated tall spruce trees growing from an underbrush of willow (*Salix* spp.) and alder (*Alnus* spp.) on an irregular, 10–15° north- east facing slope about 100 m below the contiguous treeline. A total of 26 tree-ring samples (5 mm-cores) from 25 trees were selected from the "Western Collection", a tree-ring data set that was





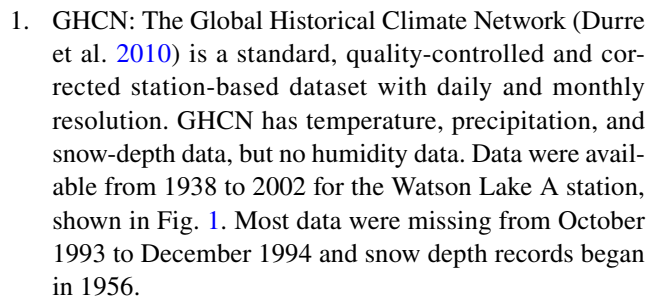
donated by Brian Luckman from the University of Western Ontario to the Tree-Ring Lab at the Lamont-Doherty Earth Observatory (LDEO) and University of Saint Andrews, UK.

The samples were scanned at a resolution of 3200 dpi using a color calibrated Epson V850 Pro scanner and the SilverFast Ai IT8 imaging software (Version 8) and the TRW were measured using the software Coorecorder 9.3 (Cybis Electronik 2019). Ring width was measured to 0.001 mm (0.0038px) precision and cross-dated against the original chronology (Morimoto 2015) to ensure accurate calendar dating using dendrochronological methods (Stokes and Smiley 1968). The 26 individual ring-width timeseries were standardized using a 200-year spline (Cook and Peters 1981) after applying a power transformation to stabilize the variance (Cook and Peters 1997). An autoregressive model was then applied to the individual standardized ring-width series to create residual ring-width timeseries. These were averaged using a robust mean with the software Arstan (Cook and Kairiukstis 1990) resulting in TRW residual chronology that emphasizes high-frequency variability.

The $\delta^{18}O_{TR}$ records were generated at LDEO following the procedures described in Andreu-Hayles et al. (2019) for cellulose extraction and the measurement of δ^{18} O using hightemperature pyrolysis in a High Temperature Conversion Elemental Analyzer (TC/EA) coupled to a Thermo Delta plus mass spectrometer. Five trees were analyzed from 1900 to 2003, a period that overlaps partially with the climate data. We selected one core sample from five individual trees mostly based on the following criteria: (1) high correlations with the master TRW chronology to be sure that they were representative of the stand; (2) trees older than 200 years to avoid potential juvenile effects; (3) visually adequate samples for wood preparation (e.g. wide rings for cutting, no locally absent rings or signs of reaction wood). Each ring was separated under a stereomicroscope using a scalpel and was analyzed individually. The resulting annual timeseries from the five individual trees were normalized and the resulting z-scores were averaged to compute a mean chronology (Fig. 2a). The Expressed Population Signal (EPS) metric was also calculated as a metric of the level of agreement among the individual trees. An EPS value exceeding the widely used threshold value of 0.85 (Wigley et al. 1984) indicates a high level of agreement among trees.

2.2 Climate data and the NASA ModelE2 isotopically-equipped climate model

We used climate data from different sources, including individual station records nearest to the study site and gridded products, each constructed differently, and which allow us to identify regional relationships between climate parameters and the tree-ring data beyond what can be detected for a single weather station. The gridded products were:



- 2. ISD: The National Centers for Environmental Information Integrated Surface Database (Smith et al. 2011) contains hourly records compiled from operational weather stations, with a more complete list of variables than GHCN. Daily maximum temperature was computed from hourly observations, and maximum daily vapor-pressure deficit (VPDMAX) was calculated from temperature and dew point temperature, which was not available in the GHCN. The data for Watson Lake were only available from July 1977 to 2002, but had good record availability during the October 1993 to December 1994 period missing from the GHCN archive for this site.
- 3. GISTEMP: The Goddard Institute for Space Studies dataset (Lenssen et al. 2019) is a gridded product of mean surface temperature (T_{surf}) anomalies going back to 1880, aggregated from different station datasets, including the GHCN. There is limited spatial interpolation, so there are large areas of missing data and higher uncertainties going back further in time.
- 4. BEST: The Berkeley Earth Surface Temperature dataset (Rohde et al. 2013) is a gridded product based on
 different station data going back to 1850, also including GHCN. The underlying data are subject to sophisticated quality control and cross-checking and there are
 separate estimates of mean daily maximum temperature
 (TMAX), daily minimum temperature (TMIN) and daily
 average temperature (TAVG) estimates. The BEST temperature fields are smoother than GISTEMP because of
 broader spatial interpolation over regions of missing station data.
- 5. UDEL precipitation: The University of Delaware global gridded precipitation product (Legates and Willmott 1990) is a spatially interpolated dataset derived from various sources of gauge data, starting with the GHCN and supplemented from other sources where GHCN data are sparse. The version 3.01 version used here is described at http://climate.geog.udel.edu/~climate/html_pages/Global2011/README.GlobalTsP2011.html
- 6. Atmospheric Reanalyses: Reanalyses products provide a complete estimate of the state of the atmosphere by combining a numerical weather prediction model and observations from different sources. This allows us to examine metrics other than surface variables such as



large-scale circulation features. In our case, we examine relationships with horizontal moisture flux, defined as the product of specific humidity (q) and the vector wind field < u,v > in the mid troposphere to identify possible source water pathways, sea-level pressure, and geopotential height (Z) in the mid-troposphere to identify possible large-scale circulation influences. Reanalyses are less suitable for analyzing relationships between local climate and tree-ring records but are the only practical means of identifying large-scale circulation influences. We used two reanalysis products to guard against product-specific interpretation of our analysis. The National Center for Environmental Prediction / National Center for Atmospheric Research reanalysis (NCEP/NCAR, Kalnay et al. 1996) is a mature, coarseresolution reanalysis going back to 1948, providing coverage for approximately half the tree-ring record, and which assimilates a broad range of surface, upper air and satellite data. For comparison, we also used the Twentieth Century Reanalysis System version 3 product (20CRv3, Slivinski et al. 2019). 20CRv3 provides coverage for the entire tree-ring record but is constrained only by surface pressure observations.

The ModelE2 GCM (Schmidt et al. 2014) is one of several GCMs equipped with stable water isotope tracers. The simulations are forced by observed, interannually-varying Sea Surface Temperatures (SSTs). Model output can be used to identify idealized climate controls on the isotopic composition of precipitation $\delta^{18}O$ over a region of interest and examine idealized relationships between climate patterns and precipitation $\delta^{18}O$ for seasons outside of the growth season.

2.3 Data analyses

We examined correlations between the Tungsten $\delta^{18}O_{TR}$ data and the aforementioned climate datasets. All of them span different periods and are constructed differently. We filtered the climate data seasonally, with the expectation that climate relationships would be most strongly affected by interannual variability during the growing season. The $\delta^{18}O_{TR}$ could also be influenced by climate during the previous winter due for example to snow δ^{18} O, spring runoff, and consequently soil moisture available for the growth season, considering that during winter the climatic influence on high-latitude precipitation δ^{18} O is more pronounced (Birks and Edwards 2009; Field et al. 2010). Large-scale climatic influences were also expected to vary seasonally because of their distinct strengths during different seasons, for example the Aleutian Low which is most strongly expressed in winter (Hartmann and Wendler 2005).

We compared the relationships of precipitation $\delta^{18}O$ with large-scale climate provided by the ModelE2 GCM versus

the relationships of $\delta^{18}O_{TR}$ with the same climate variables from reanalyses products. This comparison can help us to determine the prevailing signal in $\delta^{18}O_{TR}$ that results from strong climate influences on the $\delta^{18}O$ composition of soil water without the influence of tree physiological processes.

3 Results

3.1 Tree-ring chronologies

The Tungsten TRW chronology spans from 1584 to 2002, although replication is lower for the earlier period. EPS values in the ring width (N = 25 trees, 26 timeseries) and $\delta^{18}O_{TR}$ (N = 5 trees) chronologies (Fig. 2) exceed 0.85 from 1900 to 2002, suggesting that both tree-ring chronologies can be considered reliable for the studied period. The average of the Pearson correlation coefficient values (r) between each $\delta^{18}O_{TR}$ tree timeseries was 0.601 (p < 0.05; 1900–2003), 0.68 (p < 0.05; 1900–1969) and 0.513 (p < 0.05; 1970–2003), while the mean of the $\delta^{18}O_{TR}$ values was $19.02 \pm 0.77\%$ (1900–2003), $19.08 \pm 0.67\%$ (1900–1969) and $18.88 \pm 0.98\%$ (1970–2003). Thus, lower correlations among trees and higher Standard Deviation (SD) were found during the period 1970–2003 (r=0.513,

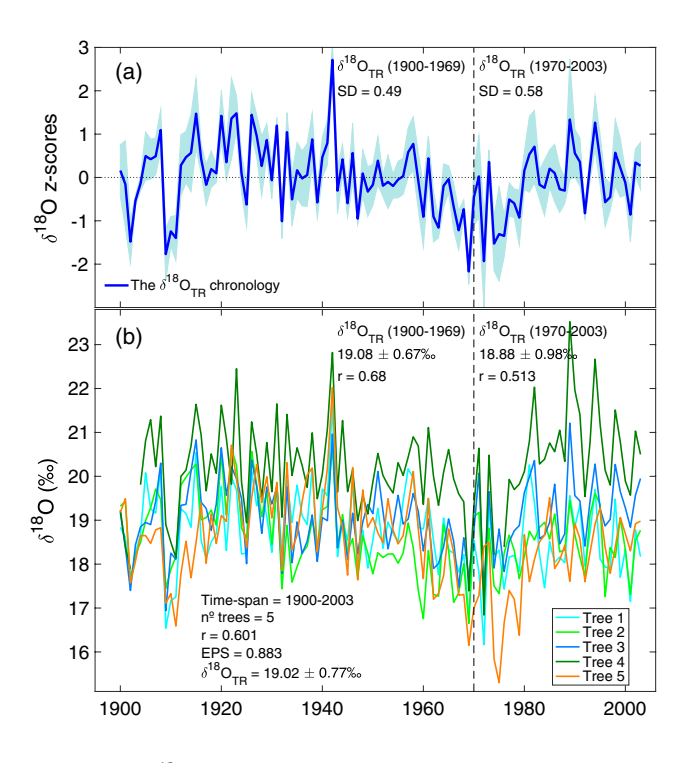


Fig. 2 a The $\delta^{18}O_{TR}$ chronology for the Tungsten site which was calculated averaging the z-scores of the $\delta^{18}O_{TR}$ individual timeseries. b The raw $\delta^{18}O_{TR}$ individual timeseries (r averaged Pearson correlation coefficient between the five trees, *EPS* Expressed Population Signal)



p<0.05 and SD=0.98‰) than during the period 1900–1969 (r=0.68, p<0.05 and SD=0.67‰). This less common variance and higher variability among trees is also shown by the higher SD of the $\delta^{18}O_{TR}$ chronology (z-scores) in the period 1970–2003 (SD=0.58) than in the period 1900–1960 (SD=0.49).

3.2 Observed climate relationships of TRW and δ¹⁸O records

Table 1 lists the Pearson's correlation coefficients between the residual TRW chronology and several climate variables for different seasons and periods of observational data availability. Over the 1977–2002 period common to both the ISD and GHCN gridded datasets, TRW was negatively correlated to spring (MAM) minimum temperature using both ISD (r=-0.48, p<0.05) and GHCN (r=-0.49, p<0.05), and positively correlated to snow depth (SNDP, r=0.64,

Table 1 Pearson's correlation coefficients (*r*) between Tungsten treering width (TRW) residual and seasonal "Watson Lake A" maximum temperature (TMAX), minimum temperature (TMIN), and maximum vapor pressure deficit (VPDMAX) from the Integrated Surface Database (ISD) over 1977–2002, and TMAX, minimum temperature (TMIN), precipitation (PREC), snowfall (SNOW), and snow depth

p < 0.05). The relationship of TRW with TMIN and SNDP were not significant over the longer 1938–2002 period, although there was a weak positive correlation (r = 0.34, p < 0.05) with summer (JJA) TMAX, and weak negative correlations with precipitation for seasons prior to the growing period, peaking at r = -0.39 for winter-spring-summer (previous DJFMAMJJA).

Table 2 lists the Pearson's correlation coefficients between the $\delta^{18}O_{TR}$ chronology and these same climate variables. VPDMAX and TMAX were positively correlated during the MAMJJA period (r=-0.86, p<0.05) and both agreed with $\delta^{18}O_{TR}$ z-scores fluctuations (Fig. 3). The $\delta^{18}O_{TR}$ z-scores showed a strong correlation with average spring–summer TMAX (Fig. 3a) from the GHCN dataset for 1938–2002 (MAMJJA, r=0.67, p<0.01), but lower correlation over the 1977–2002 period using TMAX from the ISD dataset (MAMJJA, r=0.49, p<0.05). This correlation with the spring–summer ISD TMAX was lower than when $\delta^{18}O_{TR}$

(SNDP) from the Global Historical Climate Network (GHCN) during 1977–2002 and 1938–2002. The season abbreviations are according to the first letter of the month. Seasons starting with SON and DJF begin in the previous year. Only correlations with p < 0.05 are shown. SNDP data were available only over 1956-2002

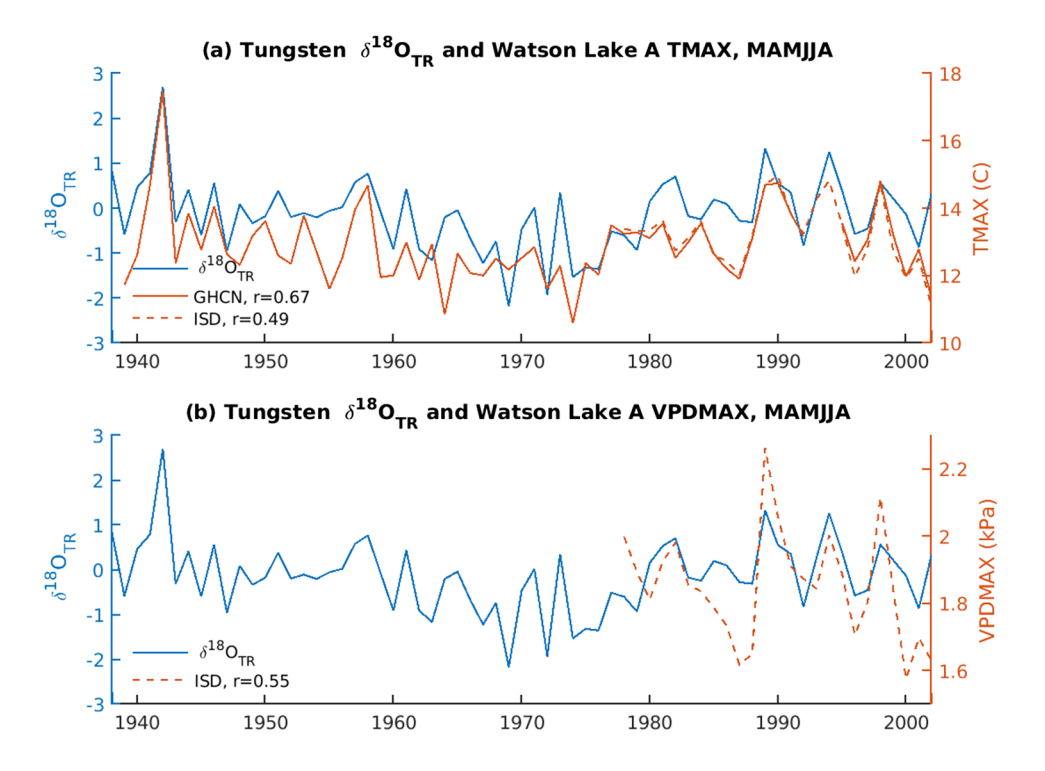
Season	ISD 1977–2002			GHCN		GHCN							
				1977–20			1938–2002						
	TMAX	TMIN	VPDMAX	TMAX	TMIN	PREC	SNOW	SNDP	TMAX	TMIN	PREC	SNOW	SNDP
JFMAMJJASOND								0.44			-0.31		
MAMJJA								0.62			-0.32		
SONDJF													
MAM		-0.48			-0.49			0.64			-0.36		
JJA									0.34				
SON													
DJF													
DJFMAMJJA		-0.45						0.58			-0.39		

Table 2 Same as Table 1, but for the $\delta^{18}O_{TR}$ z-score chronology (z-scores)

Season	ISD 1977–2002			GHCN		GHCN							
				1977–2002					1938–2002				
	TMAX	TMIN	VPDMAX	TMAX	TMIN	PREC	SNOW	SNDP	TMAX	TMIN	PREC	SNOW	SNDP
JFMAMJJASOND			0.55						0.42	0.30			
MAMJJA	0.49		0.55						0.67	0.51		-0.33	-0.34
SONDJF													
MAM									0.37	0.28		-0.31	-0.33
JJA	0.48	0.50	0.44	0.41					0.51	0.27			
SON													
DJF													
DJFMAMJJA			0.55						0.52	0.43	-0.29	-0.33	



Fig. 3 a The $\delta^{18}O_{TR}$ chronology (z-scores, blue) and average spring–summer (MAMJJA) TMAX at GHCN and ISD Watson Lake A weather station (bold and dashed orange lines, respectively), and b The $\delta^{18}O_{TR}$ chronology (z-scores, blue) and average spring–summer VPD-MAX from ISD at the same station (dashed orange line). The r indicates the Pearson correlation coefficient between the $\delta^{18}O_{TR}$ chronology and the climate timeseries



was correlated with the maximum vapor pressure deficit (VPDMAX), shown in Fig. 3b, for spring–summer (MAMJJA, $r\!=\!0.55$, $p\!<\!0.05$). While the correlations between $\delta^{18}O_{TR}$ and summer VPDMAX were significant (JJA, $r\!=\!0.44$, $p\!<\!0.05$), non-significant correlations were found with spring VPDMAX (MAM, $r\!=\!0.39$, $p\!=\!0.08$). There were also weaker positive relationships between $\delta^{18}O_{TR}$ and GHCN TMIN (MAM, $r\!=\!0.28$, $p\!<\!0.05$); JJA, $r\!=\!0.27$, $p\!<\!0.05$), although higher with ISD TMIN but only for summer (JJA, $r\!=\!0.50$, $p\!<\!0.05$) and over a shorter period. Weak negative relationships between $\delta^{18}O_{TR}$ and SNOW during spring (MAM, $r\!=\!-0.31$, $p\!<\!0.05$) slightly higher during spring–summer (MAMJJA, $r\!=\!-0.33$, $p\!<\!0.05$), as well as between $\delta^{18}O_{TR}$ SNDP (MAM, $r\!=\!-0.33$, $p\!<\!0.05$; MAMJJA, $r\!=\!-0.34$, $p\!<\!0.05$) were also found.

The GHCN TMAX correlation in summer for 1977–2002 was lower (r=0.41, p<0.05) than for the ISD data (r=0.48, p<0.05) likely because most GHCN data were missing for 1993 and 1994. Overall, the strongest correlation with $\delta^{18}O_{TR}$ was found with GHCN TMAX for spring–summer (r=0.67, p<0.01) for the whole 1938–2002 period (Fig. 3a, Table 2). The strong correlation during this season is related mainly to lower frequency changes in $\delta^{18}O$ and TMAX (Fig. 3a). Higher $\delta^{18}O_{TR}$ from 1938 until the late 1950s was associated with warmer temperatures, followed by a decrease in both from 1960 until the early 1970s, and then an increase in $\delta^{18}O_{TR}$ and summer TMAX in the late 1970s, which persisted until the early 2000s.

Based on the strength of spring and summer TMAX controls on $\delta^{18}O_{TR}$, we examined the correlations between $\delta^{18}O_{TR}$ and different gridded climate fields. Figure 4 shows the spatial field correlations between $\delta^{18}O_{TR}$ and seasonal surface temperature anomalies from BEST TMAX, GIS-TEMP T_{surf} and, for reference, the UDEL precipitation, for the period 1938-2002. For GISTEMP (Fig. 4a), there was a positive correlation pattern centered over northern British Columbia during spring-summer (MAMJJA) and extending across most of Canada. The BEST correlation field (Fig. 4c) is similar but is smoother and with higher correlations over the study site. For both GISTEMP (Fig. 4b) and BEST (Fig. 4d), there were no coherent patterns of correlation during autumn-winter (SONDJF), consistent with the analysis performed at the weather station scale. For UDEL precipitation, there were no coherent correlation patterns over the study site for either MAMJJA (Fig. 4e) or SONDJF (Fig. 4f), showing only weak negative, albeit significant, correlation in continental Canada.

To identify large-scale circulation influences, we also examined $\delta^{18}O_{TR}$ correlation fields for selected variables from the NCEP/NCAR Reanalysis I over 1948–2002 (Fig. 5). Temperature correlation maps were similar to GISTEMP and BEST and displayed a coherent region of positive correlation in western Canada during spring–summer (Fig. 5a, MAM-JJA), but no coherent pattern in autumn–winter (Fig. 5b, SONDJF). During either season, there was no coherent correlation pattern between $\delta^{18}O_{TR}$ and precipitation amount



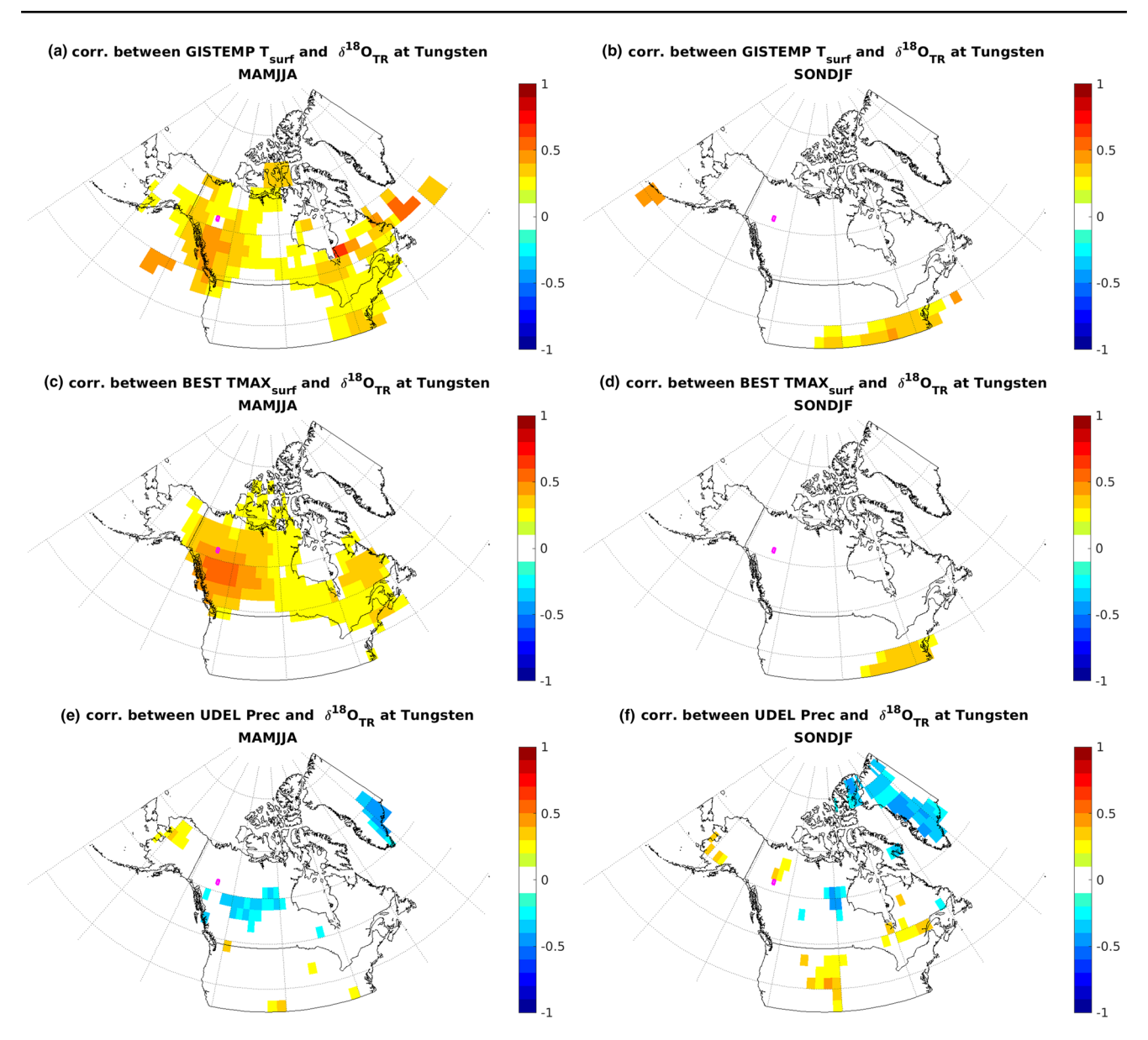


Fig. 4 Spatial field correlations between the $\delta^{18}O_{TR}$ chronology and GISTEMP surface temperature anomaly (top), BEST maximum surface temperature (middle), and University of Delaware (UDEL) precipitation (bottom) over land for spring–summer (March-August,

MAMJJA, left) and autumn-winter (September of the previous year to February (SONDJF, right), over 1938–2002. Correlations with p-values < 0.05 have been excluded. The location of the Tungsten site is shown by the small magenta box

(Fig. 5c, d). The precipitation amount correlation field was included for completeness, though we note that the NCEP reanalysis precipitation estimates are only weakly constrained by observations (Kalnay et al. 1996), unlike the corresponding UDEL precipitation used in Fig. 4e, f. There was also no apparent moisture pathway signature (Fig. 5e, f) which would have appeared as a coherent vector field in the vicinity of the study site. No clear correlation pattern was found between $\delta^{18}O_{TR}$ and SLP during either season (Fig. 5g, h). There were, however, strong correlations between $\delta^{18}O_{TR}$ and geopotential height at 500 hPa during MAMJJA (Fig. 5i), capturing the basic association

between warmer temperatures at the site and pronounced high-pressure ridging over western Canada. Individual correlation maps for spring, summer, autumn and winter were similar to the maps using 6-month season definitions for Figs. 4 (Figures S1 and S2) and 5 (Figures S3 and S4). We also compared the NCEP/NCAR 6-month correlation fields (Fig. 5) to those for the 20CRv3 reanalysis (Figure S5) for the same period 1948–2002. The region of positive correlation for MAMJJA (Figure S5a) to the southwest of the site is consistent with that for NCEP/NCAR, but it is smaller in its extent and weaker in magnitude, which was also the case for the 500 hPa geopotential height patterns (Figure S5g).



The weaker patterns in both cases are presumably due to the 20 CRv3 product having far fewer observational constraints. Using the 20 CRv3 reanalysis over the full 1900-2002 length of the $\delta^{18} O_{TR}$ record (Figure S6), there were also positive temperature (Figure S6a) and 500 hPa geopotential height patterns south of the site (Figure S6g), but which were more diffuse in their extent compared with patterns obtained using NCEP/NCAR reanalyses (Fig. 5a and 5i).

3.3 Climate-precipitation δ^{18} O relationships in GISS ModelE2 GCM

Distinct seasonal ModelE2 correlation fields of large-scale circulation features with the modelled precipitation δ^{18} O over the study site reveal different seasonal influences on source water δ^{18} O by 6-month periods (Fig. 6) and by seasons (Fig. S7 and S8). During spring-summer, the correlation pattern showed a positive relationship between precipitation δ^{18} O at the study site and temperature over northwestern North America, although with no apparent relationship in eastern Canada (Fig. 6a). These features were similar to patterns observed between $\delta^{18}O_{TR}$ and the TMAX field for the GISTEMP (Fig. 4a), BEST (Fig. 4c) and NCEP reanalysis (Fig. 5a) temperature fields. There was also pronounced positive correlation in MAMJJA between modelled precipitation δ^{18} O and TMAX in the Gulf of Alaska (Fig. 6a), seen somewhat in the GISTEMP MAMJJA correlation map with $\delta^{18}O_{TR}$ (Fig. 4a). For autumn–winter (SONDJF), there were also pronounced patterns of positive correlation between modelled precipitation δ^{18} O and TMAX (Fig. 6b), unlike the lack of relationships between $\delta^{18}O_{TR}$ and TMAX for that season when looking at the study site point scale (Fig. 4b). During spring-summer (MAMJJA), there was no apparent relationship between precipitation amount (Fig. 6c) or moisture pathway (Fig. 6e) and modelled precipitation δ^{18} O over Tungsten, consistent with the absence of any patterns in the δ¹⁸O_{TR} correlation maps (Fig. 5c, e). During autumn–winter (SONDJF), there were more coherent patterns showing a positive relationship between modelled precipitation $\delta^{18}O$ and precipitation amount in the Gulf of Alaska and negative relationship to the southeast (Fig. 6d). During the same season, higher precipitation δ^{18} O was also associated with southwesterly moisture origin (Fig. 6f). For the SLP field, no significant correlation pattern was observed during spring-summer (MAMJJA, Fig. 6g), but a strong pattern was found during autumn-winter (SONDJF, Fig. 6h) with a negative center over Alaska and the Bering Sea and a positive center over the US Great Plains. The correlation between MAMJJA precipitation δ^{18} O and 500 hPa geopotential height (Fig. 6i) were consistent with that observed for Tungsten $\delta^{18}O_{TR}$ (Fig. 5i). The correlation patterns in MAMJJA (Fig. 6i) are similar to SONDJF (Fig. 6j), but they are stronger in SONDJF.

4 Discussion

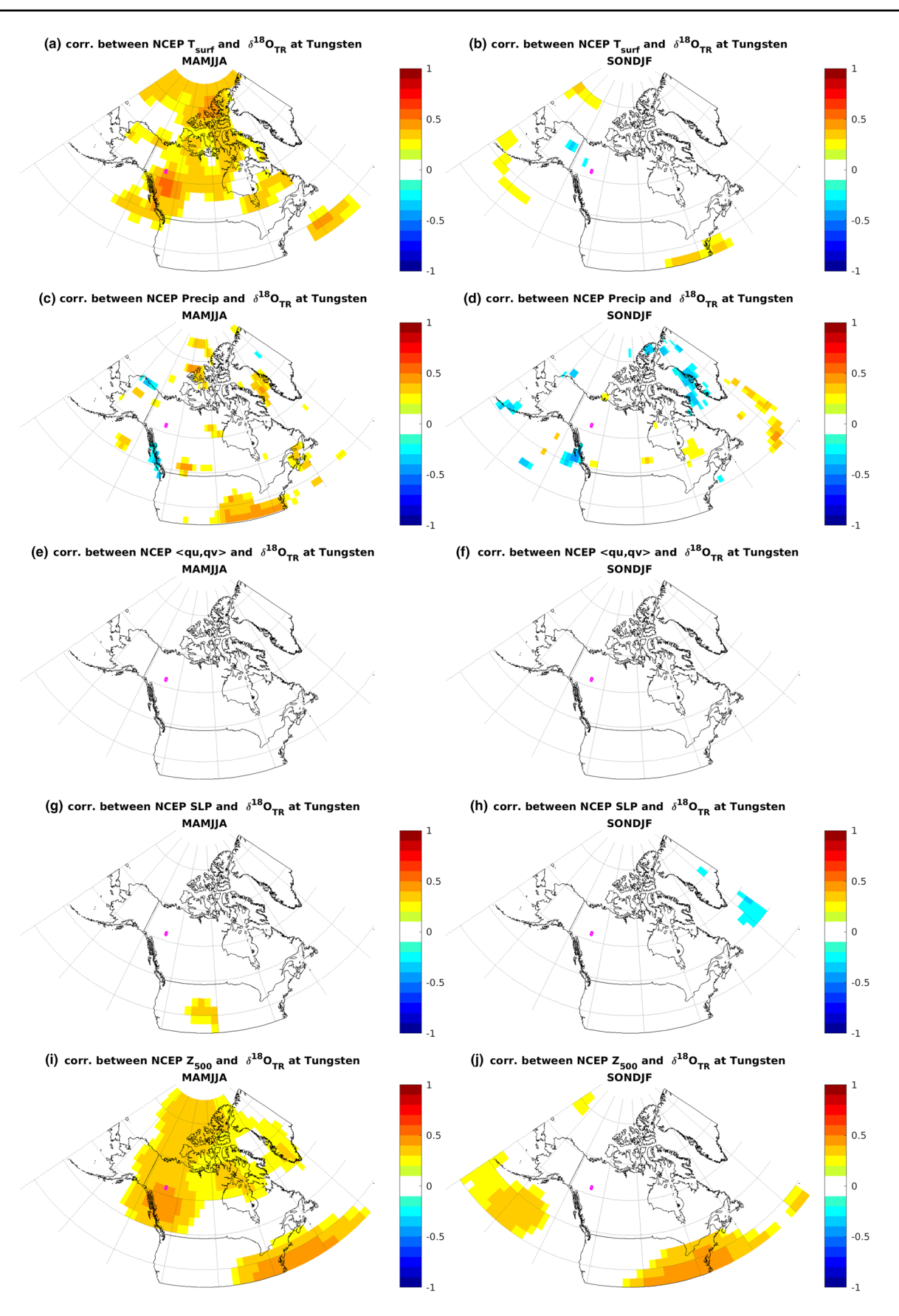
In this section, we discuss the signal and stability of the relationship between climate and the tree-ring proxies, the strong imprint of temperature in $\delta^{18}O_{TR}$ and its potential for reconstructing large-scale atmospheric patterns. For the variables considered, the climatic information contained in the TRW was weaker than in the $\delta^{18}O_{TR}$ records, but several significant relationships were identified.

4.1 Instability in the relationship between TRW and climate variables

We found a relatively unstable relationship between climatic and TRW records in some locations. For example, no significant correlation was found between TRW and summer TMAX (June to August, JJA) for the period 1977-2002, while a significant positive correlation was observed over the longer 1938–2002 period with the same dataset (GHCN). This may be related to the divergence-type phenomenon which has been well documented for a number of boreal forest sites (D'Arrigo et al. 2008; and references therein). Local site conditions, recent warming and hydroclimatic trends may also complicate the understanding of the relationship between climate and tree-ring parameters (Gedalof and Smith 2001; Li et al. 2020; Wendler et al. 2017). In the Yukon region for example, almost all of the 111 TRW chronologies from a white spruce network lost their positive relationship with summer temperatures, with one third of them showing negative responses after ~ 1950 (Morimoto 2015). A weakening of the precipitation signal and subsequent strengthening of temperature sensitivity in white spruce has been recorded in various tree-ring sites from the Alaskan and Canadian interior (Chavardes et al. 2013; Lange et al. 2020). Despite the relative instability of TRW responses in such regions, many TRW records still show strong relationships with local (Jacoby and Cook 1981), as well as largerscale temperatures and serve for north hemispheric climate reconstructions across a network of sites (D'Arrigo et al. 2014 and references therein).

Considering that cold temperatures in spring may delay the start of the growing season and reduce the period for xylogenesis in northern environments (Rossi et al. 2008), the negative correlations that we found between TRW and spring TMIN (1977–2002) are difficult to interpret. In contrast, the negative correlations between TRW and spring precipitation (1938–2002) may reflect a detrimental effect on growth because spring precipitation falling as snow could delay the start of the growing season. Vaganov et al. (1999) suggested that more abundant snow accumulation may delay snowmelt and induce a delay in cambial activity and a reduction in growth. However, other authors suggested a positive







<Fig. 5 Spatial field correlations between the $\delta^{18}O_{TR}$ chronology and NCEP surface temperature (T_{surf}), precipitation (Precip), moisture transport at 500 hPa (<qu,qv>), sea-level pressure (SLP), and geopotential height at 500 hPa (Z_{500}) for spring–summer (March-August, MAMJJA, left) and autumn–winter (September-February, SONDJF, right), over 1948–2012. Correlations with p-values < 0.05 have been excluded

role of spring snowpack on growth related to an increase in moisture availability with higher snowmelt water when the growing season starts in late spring/early summer (Yarie 2008) and/or thermal soil insulation by snow that could enhance growth (Grippa et al. 2005). In moisture-limited sites in western North America forests positive snow-growth relationships have been also reported (Coulthard et al. 2021). In the white spruce forest studied here, a positive effect of larger snowpack on tree-ring growth may be occurring although this relationship was only found in the most recent period (1977–2002).

4.2 Temperature as the dominant signal in the $\delta^{18}O_{TR}$ records

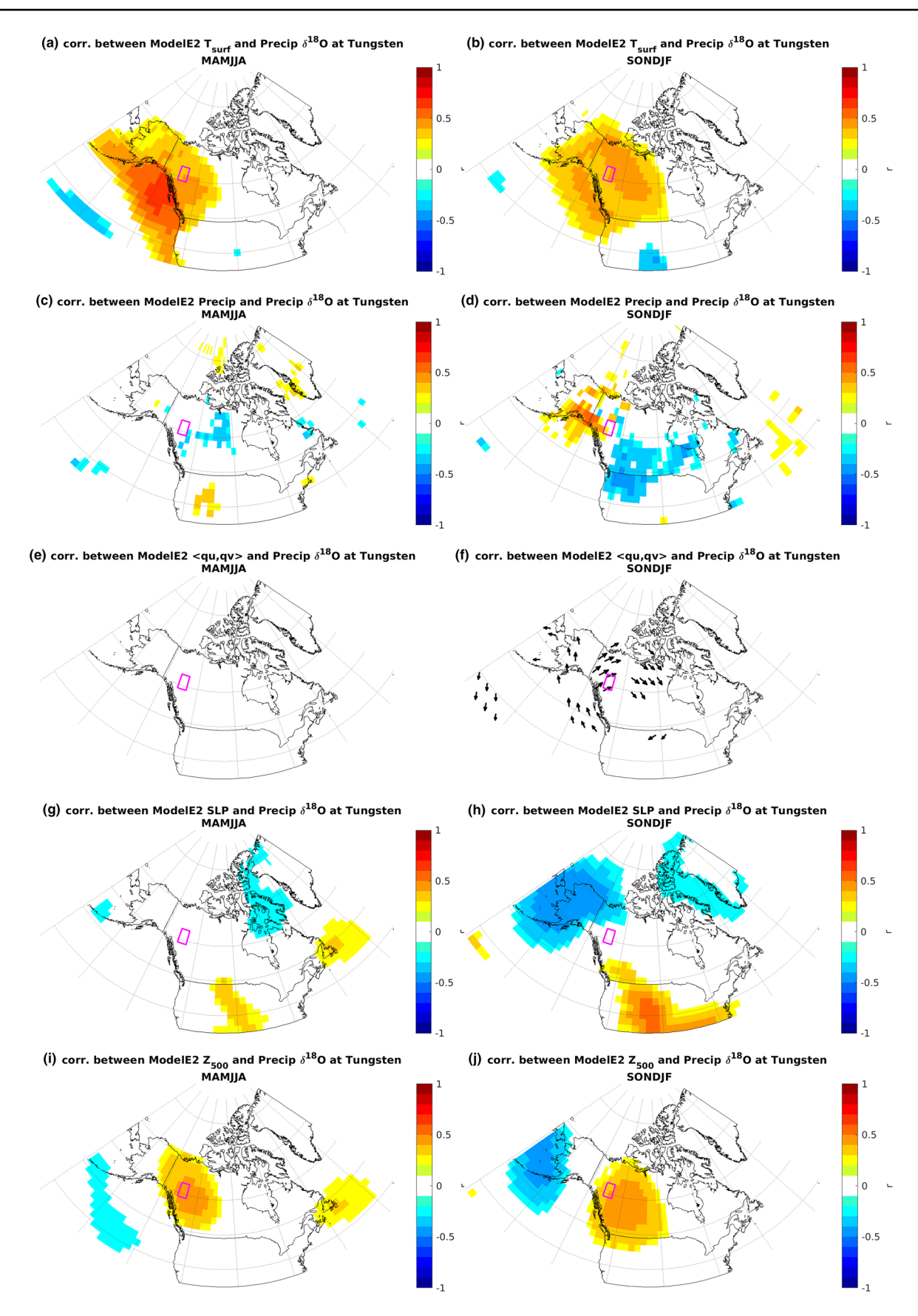
The $\delta^{18}O_{TR}$ relationships with temperature identified here were stronger and more stable throughout time than those for TRW, and broadly consistent with other studies at highlatitude North American sites. In northeastern Canada, Alvarez et al. (2018) found stronger positive correlations between $\delta^{18}O_{TR}$ and TMAX than between $\delta^{18}O_{TR}$ and TMIN. Naulier et al. (2014) found a June-July correlation of r = 0.55 (p < 0.05) with TMAX and black spruce $\delta^{18}O_{TR}$ over 1949-2005 in Quebec, slightly higher than the correlation of r = 0.45 for VPD. Using data from this site combined with a process-based model (MAIDENiso), Lavergne et al. (2017) found that the temperature signal recorded in $\delta^{18}O_{TR}$ more likely reflects the effect of temperature on isotopic enrichment of the leaf water than on the isotopic composition of the source water. Begin et al. (2015) found higher correlations between $\delta^{18}O_{TR}$ and summer VPD than for summer TMAX (r=0.64 versus r=0.55, p<0.05). In Alvarez et al. (2018), $\delta^{18}O_{TR}$ was negatively correlated with river discharge. Similarly, $\delta^{18}O_{TR}$ was negatively correlated with summer precipitation in Naulier et al. (2014) and Begin et al. (2015). We found a negative relationship between precipitation and $\delta^{18}O_{TR}$, but which was weaker and only significant during the combined winter-spring-summer seasonal period (Table 2). By contrast, Holzkamper et al. (2012) found that $\delta^{18}O_{TR}$ in white spruce was positively correlated with spring temperatures, and negatively correlated with precipitation amount at a site in north-central Canada. In northwestern North America, Porter et al. (2009) found a weak negative correlation between $\delta^{18}O_{TR}$ and April precipitation amount. Positive relationships were found between $\delta^{18}O_{TR}$ and early-spring to mid-summer minimum temperatures and

summer relative humidity, attributing the former to the temperature dependence of source water $\delta^{18}O$ and the latter to evaporative $\delta^{18}O$ enrichment. This is in agreement with our findings showing that the $\delta^{18}O_{TR}$ record was influenced by temperature variations in spring and summer. While physiological processes have most likely influenced $\delta^{18}O_{TR}$ in summer through evaporative enrichment at leaf level, spring climate also imprints $\delta^{18}O_{TR}$ potentially via temperature effects on precipitation $\delta^{18}O$ signatures (e.g. Treydte et al. 2014).

Snow plays an important role in these latitudes. A possible influence of winter snowpack on $\delta^{18}O_{TR}$ is also suggested by the negative relationships with the snow variables for the 1938–2002 period. Along with a positive correlation observed between $\delta^{18}O_{TR}$ and TMAX, Csank et al. (2016) found a negative correlation between $\delta^{18}O_{TR}$ for a site in southern Alaska and prior winter snow amount. This was consistent with our results, and possibly explained by the effects of snowpack as a moisture source during the growing season. Snow has a lower δ^{18} O than rain (Kurita et al. 2004), therefore years with greater snow accumulation would contribute to source water in the soil having lower δ^{18} O (Beria et al. 2018). However, processes operating in the opposite directions could also be taking place, weakening this negative relationship depending on the snow accumulation and residence time of the snow before melting. For example, with more snow, more snowmelt (freeze/unfreeze events), sublimation and other kinetic processes can take place leading to more ¹⁸O enrichment (Beria et al. 2018; Ebner et al. 2017).

For all tree-ring and climate parameters considered during the full 1938–2002 period of analysis, $\delta^{18}O_{TR}$ had the highest correlation (r = 0.67, p < 0.05) with spring and summer TMAX. Since $\delta^{18}O_{TR}$ is influenced by the precipitation δ^{18} O at the site via soil water, this relationship can be explained, in part, by the large-scale co-variation between temperature and δ^{18} O precipitation in northern latitudes. This occurs through a Rayleigh distillation of the water vapor that is transported by the air masses (Araguas-Araguas et al. 2000; Gat 1996). Air masses arriving with a colder history will have undergone more rainout, during which the heavier isotopologues (i.e. molecules of a particular element which differ only in the neutron number) will be removed preferentially through fractionation, leading to lower precipitation δ^{18} O at the sampling site. In addition, during condensation from water vapour to rain, more fractionation of δ^{18} O occurs under colder conditions than warmer conditions (Clark and Fritz 1997) leading to even more depleted precipitation δ^{18} O under colder conditions. Therefore, the yearly isotopic signature of precipitation δ^{18} O is the result of the variation between rainout occurrence due to colder (warmer) air masses that experience more (less) rainout events and rainouts







<Fig. 6 Spatial field correlations between annual ModelE2 precipitation δ^{18} O over the Tungsten site and surface temperature (T_{surf}), precipitation (Precip), moisture transport at 500 hPa (<qu,qv>), sealevel pressure (SLP), and geopotential height at 500 hPa (Z_{500}) for spring–summer (March-August, MAMJJA, left) and autumn–winter (September–February, SONDJF, right), over 1952–2012. Correlations with p-values < 0.05 have been excluded

with more (less) ¹⁸O fractionation associated with lower (higher) temperatures during condensation. This is manifested interannually, with lower $\delta^{18}O_{TR}$ in years with lower precipitation δ^{18} O related to colder upstream conditions (more rainout events and more ¹⁸O fractionation during condensation), while higher $\delta^{18}O_{TR}$ in years with higher precipitation $\delta^{18}O$ may be related to warmer upstream conditions (less rainout events and less ¹⁸O fractionation during condensation). Note that at high latitudes, there are not strong direct relationships between precipitation amount and precipitation $\delta^{18}O$ in the GISS GCM (Schmidt et al. 2007), measurements from the Global Network of Isotopes in Precipitation (Risi et al. 2010) or in an isotopic atmospheric water balance model (Zhang et al. 2015), even when there are positive relationships between temperature and precipitation δ^{18} O. In our study, this was seen by only weak negative correlations with GHCN precipitation during the winter-spring-summer period (Table 2) and a lack of significant correlations between the Tungsten $\delta^{18}O_{TR}$ and both the instrumental precipitation (Fig. 4e, f) and the reanalysis precipitation fields (Fig. 5c, d). In agreement, our GCM results show a lack of relationship between spring-summer modelled precipitation δ^{18} O and precipitation and over the Tungsten site (Fig. 6c, d). Note that in fall-winter higher modelled precipitation δ^{18} O was associated with more precipitation over the Gulf of Alaska and southwesterly moisture transport, which we interpret as primarily as covariation with warmer, more moist air masses arriving from the south to the Gulf of Alaska.

During the 1977–2002 period, $\delta^{18}O_{TR}$ was related to VPDMAX during the annual and combined spring / summer periods. However, the strength of these correlations was mostly driven by summer VPDMAX because non-significant correlations were found in spring alone. Thus, VPD increase may be driven by warmer summers and may induce evaporative ¹⁸O enrichment at leaf level during transpiration (Barbour 2007; Gessler et al. 2014). This is consistent with other studies in high-latitude forests of Quebec (e.g. Lavergne et al. 2017). Our GCM results relate to the idealized source water signal unaffected by tree physiological isotopic fractionation. Higher correlation between modelled δ^{18} O precipitation and temperatures were found in spring compared to summer (Fig. S7a cf. S7b). This indicates that the source water signal is stronger in spring than in summer, illustrated by the GCM diagnosis where physiological enrichment is not present but where other processes such as summer post-condensation exchange can weaken the temperature signal. Additionally, as reflected in results from observations with higher correlations between $\delta^{18}O_{TR}$ and temperature in summer than in spring (Fig. S1b cf. Fig. S1a), the temperature signal in the $\delta^{18}O_{TR}$ is higher in summer when both the source water signal and the VPD-induced ¹⁸O enrichment at leaf level are present. The strength of the δ¹⁸O_{TR}-VPDMAX relationships suggests that annual isotopic measurements in tree rings could be potentially good proxies for reconstructing summer temperature and VPD, but that analyzing earlywood and latewood isotopic measurements independently may be a better option for distinguishing the seasonality effect of source water and VPD in the $\delta^{18}O_{TR}$ signatures at a higher temporal resolution (e.g. Belmecheri et al. 2018; Levesque et al. 2017). Finally note that in the case of the study site, these data are limited by the short length of ISD data over which VPD could be calculated (compared to the longer GHCN records, for example, but which had no humidity records).

4.3 The $\delta^{18}O_{TR}$ records as a proxy for large-scale atmospheric circulation fields

The positive association between $\delta^{18}O_{TR}$ and TMAX timeseries reported is driven by both inter-annual and decadal variations in spring-summer temperature (Fig. 3). In this context, can $\delta^{18}O_{TR}$ serve as a proxy for temperature variations or even for large-scale atmospheric circulation fields? The strong $\delta^{18}O_{TR}$ -TMAX relationship was clearly seen regionally in correlation maps with GISTEMP and BEST temperature fields, with areas of higher correlation centered in northwestern North America. This was, in turn, related to a region with positive correlation with 500 hPa geopotential height centered over the study site, which we interpret as a signature of the relationship between high temperature and stronger meridional (southerly) atmospheric flow. This was similar to the patterns seen in the composite relationships between 500 hPa geopotential height and precipitation δ^{18} O at three sites in central Canada (Birks and Edwards 2009). These relationships between $\delta^{18}O_{TR}$, surface temperature and geopotential height were also seen in those between modelled precipitation δ^{18} O over the study site, surface temperature and geopotential height in the NASA GISS ModelE2 simulations. In the model simulations, these relationships were seen for both the spring-summer (MAMJJA) and fall-winter (SONDJF), unlike the $\delta^{18}O_{TR}$ for which positive correlations were only seen during the MAMJJA period more associated with the growing season. Similarly, for precipitation amount and moisture transport, coherent positive associations between precipitation δ^{18} O and southwesterly moisture transport were only seen in model simulations for the SONDJF period; their absence in the $\delta^{18}O_{TR}$ can



be explained by weaker circulation features during the spring-summer when trees are growing. The wintertime correlation patterns in SLP and Z₅₀₀ fields are reminiscent of the Pacific North America (PNA) pattern (Barnston and Livezev 1987). Over southern North America, Liu et al. (2014) found a positive to negative dipole correlation pattern between the PNA index and modeled winter precipitation δ^{18} O (Yoshimura et al. 2008), oriented southeastward from western Canada which is consistent with the spatial pattern observed in Fig. 6j. This suggests that previous reconstructions of the PNA using tree-ring width records (Liu et al. 2017) could be enhanced with isotopic measurements to further understand hydroclimatic relationships and external forcing over North America throughout the last millennium. Our results also suggest that combining $\delta^{18}O_{TR}$, which is most sensitive to summertime circulation, with other isotopic archives more sensitive to wintertime circulation such as ice cores (Field et al. 2010) have potential for annual or seasonally-varying reconstructions of atmospheric circulation.

4.4 The potential role of the Pacific Ocean forcing

Changes in the relationships between climate and both TRW and $\delta^{18}O_{TR}$ records over the 1938–2002 period can be in part driven by a regional climate shift in the mid-1970s. After 1977 TRW became insensitive to the previous positive role of summer temperatures, negatively influenced by TMIN and positively by snow depth, while $\delta^{18}O_{TR}$ became more strongly linked to TMAX and insensitive to the previously negative influence of snow depth. We also observed less common shared variance and higher variability in $\delta^{18}O_{TR}$ among the trees after 1970 (Fig. 2). The increase in temperature and $\delta^{18}O_{TR}$ variability during this period is consistent with an abrupt shift towards higher mean annual observed temperature in interior Alaska (Hartmann and Wendler 2005) and a broad range of environmental changes (Ebbesmeyer et al. 1991; Mantua et al. 1997). These were concordant to the well-known regime shift of the Pacific Decadal Oscillation (PDO) in 1976/77 from its negative (cold) to positive (warm) phase (Ebbesmeyer et al. 1991; Mantua et al. 1997; Trenberth and Hurrell 1994) and of the PNA Pattern index to its positive phase (Minobe and Mantua 1999; Overland et al. 1999), both associated with a strengthening of the Aleutian Low. Such apparent readjustment of largescale mode of climate variability was also seen in $\delta^{18}O_{TR}$ records for the Mackenzie Delta, NWT (Porter et al. 2014), and in δ^{18} O data from the Mt. Logan ice core (Field et al. 2010). These observations are consistent with the broader regional footprint of TMAX in our $\delta^{18}O_{TR}$ chronology, seen in the correlation patterns with the GISTEMP and BEST gridded temperature products (Fig. 4). It is also interesting to note that similar weakness in the strength of the relationship between $\delta^{18}O_{TR}$ and temperatures have also been observed after 1970 in the extra-tropics in Patagonia, South America (Lavergne et al. 2016), reinforcing the hypothesis that our observations may be related to changes in the PDO and its impact in driving inter-hemispheric ocean-atmospheric connections across both of the Western Americas (Villalba et al. 2011).

5 Conclusions

Here, we investigated the potential of tree-ring isotopic and ring-width measurements of white spruce at the boreal forest treeline in the Northwest Territories, Canada to record local to regional climate and reconstruct atmospheric circulation patterns. Among the relationships examined, the strongest was a temperature signal imprinted in $\delta^{18}O_{TR}$ cellulose at the Tungsten site over 1938-2002, likely driven by the precipitation δ^{18} O signature (i.e. source water). This was seen consistently comparing $\delta^{18}O_{TR}$ with temperature data from different sources, i.e. a weather station, two gridded temperature products, and two reanalyses. The imprint of temperature on $\delta^{18}O_{TR}$ is likely associated to the temperature impact on fractionation processes during the condensation of water vapor to rainwater expected in this high latitude (i.e. colder upstream conditions, more rainout events and more ¹⁸O fractionation during condensation leading to lower precipitation δ^{18} O). Evaporative enrichment of 18 O at leaf level could also contributing to the final $\delta^{18}O_{TR}$ signature, but mainly during summer. We also found a weak but significant negative relationship between snow accumulation and $\delta^{18}O_{TR}$ over the 1983–2002 period; a deeper snowpack leads to a greater supply of soil water with lower δ^{18} O values.

Diagnosis with an isotopically-equipped climate model contributed to our understanding of seasonal differences in the influence of temperature and circulation patterns on the $\delta^{18}O_{TR}$ without the influence of tree physiology. No significant relationships were found between the $\delta^{18}O_{TR}$ and reanalysis moisture transport for either fall-winter or spring-summer, but appeared during fall-winter, if unevenly, for the modelled precipitation $\delta^{18}O$ at the sampling site. Our interpretation is that the fall-winter circulation controls on precipitation $\delta^{18}O$ are not strong enough to influence tree uptake of isotopically depleted water during the spring and summer growth season, despite a possible relationship between winter snow depth and $\delta^{18}O_{TR}$.

We conclude that the $\delta^{18}O_{TR}$ records for northwestern Canada reflect the spring–summer atmospheric circulation patterns in this region. The broad consistency of the positive relationships between $\delta^{18}O_{TR}$ and temperature observed in this study and across northern North America demonstrates the potential of using stable oxygen isotopes measured in tree rings for reconstructing temperature, but also other



large-scale climate indicators as a novel aspect. Combining the isotopic and other climate signals gleaned from various tree-ring parameters (e.g., MXD, BI) we could produce more robust climate reconstructions. As with dendroclimatological studies from tree-ring width at multiple sites, we therefore expect further gains in reconstructions using a multispecies network (Pederson et al. 2013) of tree-ring isotopic records at regional, continental and eventually hemispheric scales. Forward modeling of tree-ring parameters, as in Lavergne et al. (2017), will further help to understand the relative contributions of 'site-level' factors such as source water uptake and leaf-level processes to better isolate past signals of temperature and moisture variability.

Supplementary Information The online version contains supplementary material available at https://doi.org/10.1007/s00382-021-05932-4.

Acknowledgements This research was supported by a Lamont-Doherty Earth Observatory Climate Center grant and by US National Science Foundation (NSF) Grants PLR-1504134, PLR-1603473, AGS-1502150 and OISE-1743738. A.L. was supported by a Marie Sklodowska-Curie Individual Fellowship under the European Union's Horizon 2020 Research and Innovation Programme (Grant Agreement No: 838739 ECAW-ISO). F.G. was supported by the NSERC Discovery Grant RGPIN-2021-03553. We are thankful to Wei Huang from the Stable Isotope Laboratory for their support on isotopic measurements at the Lamont-Doherty Earth Observatory.

Author contributions RDF and LA-H design the study, conducted the analyses and wrote the manuscript with contributions from all authors. BHL and DM collected the samples and generated the reference treering width chronology. LA-H and RO generated the isotopic chronology at the Lamont-Doherty Earth Observatory of Columbia University.

Funding This research was supported by a Lamont-Doherty Earth Observatory Climate Center grant and by US National Science Foundation (NSF) Grants PLR-1504134, PLR-1603473, AGS-1502150 and OISE-1743738.

Availability of data and material The data that support the findings of this study are available from the ITRDB database at the NOAA server (link) and Arctic Data Center (ADC).

Code availability All code will be made publicly available should the paper be accepted for publication.

Declarations

Conflict of interest The authors have no relevant financial or non-financial interests to disclose.

Ethics approval This paper is in compliance with Ethical Standard.

Consent to participate All authors consent to participate in this paper.

Consent for publication All authors consent for publication of the submitted manuscript.

References

- AB CED (2019) CooRecorder basics http://www.cybis.se/forfun/dendro/helpcoorecorder7/index.php. (Accessed Mar 2020)
- Alvarez C, Begin C, Savard MM, Dinis L, Marion J, Smirnoff A, Begin Y (2018) Relevance of using whole-ring stable isotopes of black spruce trees in the perspective of climate reconstruction. Dendrochronologia 50:64–69. https://doi.org/10.1016/j.dendro.2018. 05.004
- Anchukaitis KJ et al (2012) Tree-ring-reconstructed summer temperatures from Northwestern North America during the Last Nine Centuries. J Clim 26:3001–3012. https://doi.org/10.1175/jcli-d-11-00139.1
- Anchukaitis KJ et al (2017) Last millennium Northern Hemisphere summer temperatures from tree rings: part II, spatially resolved reconstructions. Quat Sci Rev 163:1–22. https://doi.org/10.1016/j.quascirev.2017.02.020
- Andreu-Hayles L, D'Arrigo R, Anchukaitis KJ, Beck PSA, Frank D, Goetz S (2011a) Varying boreal forest response to Arctic environmental change at the Firth River. Alaska. Environ Res Lett 6:045503
- Andreu-Hayles L, Planells O, Gutiérrez E, Muntan E, Helle G, Anchukaitis KJ, Schleser GH (2011b) Long tree-ring chronologies reveal 20th century increases in water-use efficiency but no enhancement of tree growth at five Iberian pine forests. Global Change Biol 17:2095–2112. https://doi.org/10.1111/j.1365-2486.2010.02373.x
- Andreu-Hayles L et al (2017) 400 Years of summer hydroclimate from stable isotopes in Iberian trees. Clim Dyn 49:143–161. https://doi.org/10.1007/s00382-016-3332-z
- Andreu-Hayles L et al (2019) A high yield cellulose extraction system for small whole wood samples and dual measurement of carbon and oxygen stable isotopes. Chem Geol 504:53–65. https://doi.org/10.1016/j.chemgeo.2018.09.007
- Araguas-Araguas L, Froehlich K, Rozanski K (2000) Deuterium and oxygen-18 isotope composition of precipitation and atmospheric moisture. Hydrol Process 14:1341–1355. https://doi.org/10.1002/1099-1085(20000615)14:8%3c1341::Aid-hyp983%3e3.0.
- Balting DF et al (2021) Large-scale climate signals of a European oxygen isotope network from tree rings. Clim past 17:1005–1023. https://doi.org/10.5194/cp-17-1005-2021
- Barber VA, Juday GP, Finney BP (2000) Reduced growth of Alaskan white spruce in the twentieth century from temperature-induced drought stress. Nature 405:668–673
- Barbeta A et al (2020) Evidence for distinct isotopic composition of sap and tissue water in tree stems: consequences for plant water source identification. bioRxiv. https://doi.org/10.1101/2020.06. 18.160002
- Barbour MM (2007) Stable oxygen isotope composition of plant tissue: a review. Funct Plant Biol 34:83–94. https://doi.org/10.1071/FP06228
- Barnston AG, Livezey RE (1987) Classification, seasonality and persistence of low-frequency atmospheric circulation patterns. Mon Weather Rev 115:1083–1126. https://doi.org/10.1175/1520-0493(1987)115%3c1083:csapol%3e2.0.co;2
- Begin C, Gingras M, Savard MM, Marion J, Nicault A, Begin Y (2015) Assessing tree-ring carbon and oxygen stable isotopes for climate reconstruction in the Canadian northeastern boreal forest. Palaeogeogr Palaeoclimatol Palaeoecol 423:91–101. https://doi.org/10. 1016/j.palaeo.2015.01.021
- Belmecheri S, Wright WE, Szejner P, Morino KA, Monson RK (2018) Carbon and oxygen isotope fractionations in tree rings reveal



interactions between cambial phenology and seasonal climate. Plant Cell Environ 41:2758–2772. https://doi.org/10.1111/pce. 13401

- Beria H, Larsen JR, Ceperley NC, Michelon A, Vennemann T, Schaefli B (2018) Understanding snow hydrological processes through the lens of stable water isotopes WIREs. Water 5:e1311. https://doi.org/10.1002/wat2.1311
- Birks SJ, Edwards TWD (2009) Atmospheric circulation controls on precipitation isotope-climate relations in western Canada. Tellus Ser B 61:566–576. https://doi.org/10.1111/j.1600-0889.2009.
- Briffa KR, Osborn TJ, Schweingruber FH (2004) Large-scale temperature inferences from tree rings: a review. Global Planet Change 40:11–26. https://doi.org/10.1016/s0921-8181(03)00095-x
- Brigode P, Brissette F, Nicault A, Perreault L, Kuentz A, Mathevet T, Gailhard J (2016) Streamflow variability over the 1881–2011 period in northern Quebec: comparison of hydrological reconstructions based on tree rings and geopotential height field reanalysis. Clim past 12:1785–1804. https://doi.org/10.5194/cp-12-1785-2016
- Brinkmann N, Seeger S, Weiler M, Buchmann N, Eugster W, Kahmen A (2018) Employing stable isotopes to determine the residence times of soil water and the temporal origin of water taken up by *Fagus sylvatica* and *Picea abies* in a temperate forest. New Phytol 219:1300–1313. https://doi.org/10.1111/nph.15255
- Cernusak LA et al (2016) Stable isotopes in leaf water of terrestrial plants. Plant Cell Environ 39:1087–1102. https://doi.org/10.1111/pce.12703
- Chavardes RD, Daniels LD, Waeber PO, Innes JL, Nitschke CR (2013) Unstable climate-growth relations for white spruce in southwest Yukon, Canada. Clim Change 116:593–611. https://doi.org/10.1007/s10584-012-0503-8
- Clark ID, Fritz P (1997) Environmental isotopes in hydrogeology, 1st edn. Lewis Publishers. https://doi.org/10.1201/9781482242911
- Cook ER, Kairiukstis LA (1990) Methods of dendrochronology applications in the environmental sciences. In: Cook ER, Kairiukstis L. a. (eds) Methods of dendrochronology: applications in the environmental sciences. Xii+394p. Kluwer Academic Publishers: Dordrecht, Netherlands; Boston, Massachusetts, USA. Illus. Maps, XII+394P-XII+394P
- Cook ER, Peters K (1981) The smoothing spline: a new approach to standardizing forest interior tree-ring width series for dendroclimatic studies Tree-Ring. Bulletin 41:45–53
- Cook ER, Peters K (1997) Calculating unbiased tree-ring indices for the study of climatic and environmental change. Holocene 7:359–368
- Coulthard BL, Anchukaitis KJ, Pederson GT, Cook E, Littell J, Smith DJ (2021) Snowpack signals in North American tree rings. Environ Res Lett 16:034037. https://doi.org/10.1088/1748-9326/abd5de
- Csank AZ, Fortier D, Leavitt SW (2013) Annually resolved temperature reconstructions from a late Pliocene–early Pleistocene polar forest on Bylot Island, Canada. Palaeogeogr Palaeoclimatol Palaeoecol 369:313–322. https://doi.org/10.1016/j.palaeo.2012.10.040
- Csank AZ, Miller AE, Sherriff RL, Berg EE, Welker JM (2016) Treering isotopes reveal drought sensitivity in trees killed by spruce beetle outbreaks in south-central Alaska. Ecol Appl 26:2001–2020. https://doi.org/10.1002/eap.1365
- Dansgaard W (1964) Stable isotopes in precipitation. Tellus 16:436–468
- D'Arrigo R, Villalba R, Wiles G (2001) Tree-ring estimates of Pacific decadal climate variability. Clim Dyn 18:219–224. https://doi.org/10.1007/s003820100177
- D'Arrigo R, Wilson R, Liepert B, Cherubini P (2008) On the "divergence problem" in northern forests: a review of the tree-ring

- evidence and possible causes. Global Planet Change 60:289–305. https://doi.org/10.1016/j.gloplacha.2007.03.004
- D'Arrigo R et al (2014) Temperature Reconstructions for the Northern Hemisphere. Dendro Climatic Stud 67:23–35
- Durre I, Menne MJ, Gleason BE, Houston TG, Vose RS (2010) Comprehensive automated quality assurance of daily surface observations. J Appl Meteorol Climatol 49:1615–1633. https://doi.org/10.1175/2010jamc2375.1
- Ebbesmeyer CC, Cayan DR, Milan DR, Nichols FH, Peterson DH, Redmond KT (1991) 1976 step in the Pacific climate: forty environmental changes between 1968–1975 and 1977–1984. pp 115–126. In: Betancourt JL, Tharp VL (eds) Proceedings of the 7th Annual Climate (PACLIM) Workshop, April 1990, California Department of Water Resources, Interagency Ecological Studies Program Technical Report 26
- Ebner PP, Steen-Larsen HC, Stenni B, Schneebeli M, Steinfeld A (2017) Experimental observation of transient δ^{18} O interaction between snow and advective airflow under various temperature gradient conditions. Cryosphere 11:1733–1743. https://doi.org/10.5194/tc-11-1733-2017
- Field RD, Moore GWK, Holdsworth G, Schmidt GA (2010) A GCM-based analysis of circulation controls on delta O-18 in the southwest Yukon, Canada: Implications for climate reconstructions in the region. Geophys Res Lett. https://doi.org/10.1029/2009g 1041408
- Gaglioti BV et al (2019) Traumatic Resin Ducts in Alaska mountain Hemlock trees provide a new proxy for winter storminess. J Geophys Res-Biogeosci 124:1923–1938. https://doi.org/10.1029/2018jg004849
- Gat JR (1996) Oxygen and hydrogen isotopes in the hydrologic cycle. Annu Rev Earth Planet Sci 24:225–262. https://doi.org/10.1146/annurev.earth.24.1.225
- Gedalof Z, Smith DJ (2001) Interdecadal climate variability and regime-scale shifts in Pacific North America. Geophys Res Lett 28:1515–1518. https://doi.org/10.1029/2000gl011779
- Gennaretti F, Huard D, Naulier M, Savard M, Begin C, Arseneault D, Guiot J (2017) Bayesian multiproxy temperature reconstruction with black spruce ring widths and stable isotopes from the northern Quebec taiga. Clim Dyn 49:4107–4119. https://doi.org/10.1007/s00382-017-3565-5
- Gessler A, Pedro Ferrio J, Hommel R, Treydte K, Werner RA, Monson RK (2014) Stable isotopes in tree rings: towards a mechanistic understanding of isotope fractionation and mixing processes from the leaves to the wood. Tree Physiol 34:796–818. https://doi.org/10.1093/treephys/tpu040
- Grippa M, Kergoat L, Le Toan T, Mognard NM, Delbart N, L'Hermitte J, Vicente-Serrano SM (2005) The impact of snow depth and snowmelt on the vegetation variability over central Siberia. Geophys Res Lett. https://doi.org/10.1029/2005GL0242
- Hartmann B, Wendler G (2005) The significance of the 1976 pacific climate shift in the climatology of Alaska. J Clim 18:4824–4839. https://doi.org/10.1175/jcli3532.1
- Holzkamper S, Tillman PK, Kuhry P, Esper J (2012) Comparison of stable carbon and oxygen isotopes in *Picea glauca* tree rings and Sphagnum fuscum moss remains from subarctic Canada. Quatern Res 78:295–302. https://doi.org/10.1016/j.yqres.2012.05.014
- Jacoby GC, Cook ER (1981) Past temperature-variations inferred from a 400-year tree-ring chronology from Yukon-territory, Canada. Arctic Alpine Res 13:409–418. https://doi.org/10.2307/1551051
- Kalnay E et al (1996) The NCEP/NCAR 40-year reanalysis project. Bull Am Meteorol Soc 77:437–471. https://doi.org/10.1175/1520-0477(1996)077%3c0437:tnyrp%3e2.0.co;2



- Kurita N, Yoshida N, Inoue G, Chayanova EA (2004) Modern isotope climatology of Russia: a first assessment. J Geophys Res-Atmos. https://doi.org/10.1029/2003jd003404
- Lange J, Carrer M, Pisaric MFJ, Porter TJ, Seo J-W, Trouillier M, Wilmking M (2020) Moisture-driven shift in the climate sensitivity of white spruce xylem anatomical traits is coupled to largescale oscillation patterns across northern treeline in northwest North America. Glob Change Biol 26:1842–1856. https://doi.org/ 10.1111/gcb.14947
- Lavergne A, Daux V, Villalba R, Pierre M, Stievenard M, Vimeux F, Srur AM (2016) Are the oxygen isotopic compositions of *Fitzroya* cupressoides and *Nothofagus pumilio* cellulose promising proxies for climate reconstructions in northern Patagonia? J Geophys Res-Biogeosci 121:767–776. https://doi.org/10.1002/2015jg003260
- Lavergne A et al (2017) Modelling tree ring cellulose delta O-18 variations in two temperature-sensitive tree species from North and South America. Clim past 13:1515–1526. https://doi.org/10.5194/cp-13-1515-2017
- Legates DR, Willmott CJ (1990) Mean seasonal and spatial variability in gauge-corrected, global precipitation. Int J Climatol 10:111–127. https://doi.org/10.1002/joc.3370100202
- Lenssen NJL, Schmidt GA, Hansen JE, Menne MJ, Persin A, Ruedy R, Zyss D (2019) Improvements in the GISTEMP uncertainty model. J Geophys Res-Atmos 124:6307–6326. https://doi.org/10.1029/2018jd029522
- Levesque M, Andreu-Hayles L, Pederson N (2017) Water availability drives gas exchange and growth of trees in northeastern US, not elevated CO₂ and reduced acid deposition. Sci Rep 7:9. https://doi.org/10.1038/srep46158
- Li SJ et al (2020) The Pacific Decadal Oscillation less predictable under greenhouse warming. Nat Clim Change 10:30. https://doi.org/10.1038/s41558-019-0663-x
- Liu Z, Yoshmura K, Bowen GJ, Welker JM (2014) Pacific-North American teleconnection controls on precipitation isotopes (delta O-18) across the Contiguous United States and adjacent regions: a GCM-based analysis. J Clim 27:1046–1061
- Liu ZF, Tang YL, Jian ZM, Poulsen CJ, Welker JM, Bowen GJ (2017) Pacific North American circulation pattern links external forcing and North American hydroclimatic change over the past millennium. Proc Natl Acad Sci USA 114:3340–3345. https://doi.org/ 10.1073/pnas.1618201114
- Mantua NJ, Hare SR, Zhang Y, Wallace JM, Francis RC (1997) A pacific interdecadal climate oscillation with impacts on salmon production. Bull Am Meteorol Soc 78:1069–1079
- McCarroll D, Loader NJ (2004) Stable isotopes in tree rings. Quat Res Rev 23:771–801
- Minobe S, Mantua N (1999) Interdecadal modulation of interannual atmospheric and oceanic variability over the North Pacific. Prog Oceanogr 43:163–192. https://doi.org/10.1016/S0079-6611(99) 00008-7
- Morimoto DS (2015) Dendroclimatic studies of white spruce in the Yukon Territory, Canada, Electronic Thesis and Dissertation Repository. 2991. https://ir.lib.uwo.ca/etd/2991
- Naulier M, Savard MM, Begin C, Marion J, Arseneault D, Begin Y (2014) Carbon and oxygen isotopes of lakeshore black spruce trees in northeastern Canada as proxies for climatic reconstruction. Chem Geol 374:37–43. https://doi.org/10.1016/j.chemgeo. 2014 02 031
- Naulier M et al (2015) A millennial summer temperature reconstruction for northeastern Canada using oxygen isotopes in Subfossil Trees. Clim past 11:1153–1164. https://doi.org/10.5194/cp-11-1153-2015
- Overland JE, Adams JM, Bond NA (1999) Decadal variability of the aleutian low and its relation to high-latitude circulation. J Clim 12:1542–1548. https://doi.org/10.1175/1520-0442(1999)012% 3c1542:Dvotal%3e2.0.Co;2

- Pederson N et al (2013) Is an epic pluvial masking the water insecurity of the greater New York city region? J Clim 26:1339–1354. https://doi.org/10.1175/jcli-d-11-00723.1
- Porter TJ, Pisaric MFJ, Kokelj SV, Edwards TWD (2009) Climatic signals in delta C-13 and delta O-18 of Tree-rings from White Spruce in the Mackenzie Delta Region, Northern Canada. Arctic Antarctic Alpine Res 41:497–505. https://doi.org/10.1657/1938-4246-41.4.497
- Porter TJ et al (2014) Spring-summer temperatures since AD 1780 reconstructed from stable oxygen isotope ratios in white spruce tree-rings from the Mackenzie Delta, northwestern Canada. Clim Dyn 42:771–785. https://doi.org/10.1007/s00382-013-1674-3
- Risi C, Bony S, Vimeux F, Jouzel J (2010) Water-stable isotopes in the LMDZ4 general circulation model: model evaluation for presentday and past climates and applications to climatic interpretations of tropical isotopic records. J Geophys Res Atmos 115
- Rohde R et al (2013) A new estimate of the average earth surface land temperature spanning 1753 to 2011. Geoinform Geostat. https://doi.org/10.4172/2327-4581.1000101
- Rossi S et al (2008) Critical temperatures for xylogenesis in conifers of cold climates. Global Ecol Biogeography 17:696–707
- Schmidt GA, LeGrande AN, Hoffmann G (2007) Water isotope expressions of intrinsic and forced variability in a coupled ocean-atmosphere model. J Geophys Res Atmos 112
- Schmidt GA et al (2014) Configuration and assessment of the GISS ModelE2 contributions to the CMIP5 archive. J Adv Model Earth Syst 6:141–184. https://doi.org/10.1002/2013ms000265
- Slivinski LC et al (2019) Towards a more reliable historical reanalysis: improvements for version 3 of the twentieth century reanalysis system. Quart J R Meteorol Soc 145:2876–2908. https://doi.org/10.1002/qj.3598
- Smith A, Lott N, Vose R (2011) The integrated surface database recent developments and partnerships. Bull Am Meteor Soc 92:704–708. https://doi.org/10.1175/2011bams3015.1
- Stokes M, Smiley T (1968) An introduction to tree-ring dating. University of Chicago Press, Chicago, p 73
- Szejner P et al (2016) Latitudinal gradients in tree ring stable carbon and oxygen isotopes reveal differential climate influences of the north American monsoon system. J Geophys Res-Biogeosci 121:1978–1991. https://doi.org/10.1002/2016jg003460
- Trenberth KE, Hurrell JW (1994) Decadal atmosphere-ocean variations in the Pacific. Clim Dyn 9:303–319. https://doi.org/10.1007/bf00204745
- Treydte K et al (2014) Seasonal transfer of oxygen isotopes from precipitation and soil to the tree ring: source water versus needle water enrichment. New Phytol 202:772–783. https://doi.org/10.1111/nph.12741
- Vaganov EA, Hughes MK, Kirdyanov AV, Schweingruber FH, Silkin PP (1999) Influence of snowfall and melt timing on tree growth in subarctic Eurasia. Nature 400:149-151
- Villalba R et al (2011) Dendroclimatology from regional to continental scales: understanding regional processes to reconstruct large-scale climatic variations across the western Americas. In: Hughes MK, Swetnam TW, Diaz HF (eds) Dendroclimatology, vol 11. Developments in paleoenvironmental research. Springer, Netherlands, pp 175–227. https://doi.org/10.1007/978-1-4020-5725-0_7
- Wendler G, Gordon T, Stuefer M (2017) On the Precipitation and Precipitation Change in Alaska. Atmosphere. https://doi.org/10.3390/atmos8120253
- Wigley TML, Briffa KR, Jones PD (1984) On the average value of correlated time-series, with applications in dendroclimatology and hydrometeorology. J Clim Appl Meteorol 23:201–213
- Wilson RJS, Luckman BH (2003) Dendroclimatic reconstruction of maximum summer temperatures from upper treeline sites in Interior British Columbia, Canada. Holocene 13:851–861. https://doi. org/10.1191/0959683603h1663rp



- Wilson R et al (2016) Last millennium northern hemisphere summer temperatures from tree rings: part I: the long term context. Quatern Sci Rev 134:1–18. https://doi.org/10.1016/j.quascirev.2015. 12.005
- Wilson R, D'Arrigo R, Andreu-Hayles L, Oelkers R, Wiles G, Anchukaitis K, Davi N (2017) Experiments based on blue intensity for reconstructing north pacific temperatures along the Gulf of Alaska. Clim past 13:1007–1022. https://doi.org/10.5194/cp-13-1007-2017
- Wilson R et al (2019) Improved dendroclimatic calibration using blue intensity in the southern Yukon. Holocene. https://doi.org/10. 1177/0959683619862037
- Yarie J (2008) Effects of moisture limitation on tree growth in upland and floodplain forest ecosystems in interior Alaska. For Ecol

- Manage 256:1055–1063. https://doi.org/10.1016/j.foreco.2008. 06.022
- Yoshimura K, Kanamitsu M, Noone D, Oki T (2008) Historical isotope simulation using reanalysis atmospheric data. J Geophys Res Atmos 113
- Zhang XP, Guan HD, Zhang XZ, Wu HW, Li G, Huang YM (2015) Simulation of stable water isotopic composition in the atmosphere using an isotopic atmospheric water balance model. Int J Climatol 35:846–859. https://doi.org/10.1002/joc.4019

Publisher's Note Springer Nature remains neutral with regard to jurisdictional claims in published maps and institutional affiliations.

